Chapter 9
Dielectric-Modulated Biosensor Based on Vertical Tunnel Field-Effect Transistor

Vandana Devi Wangkheirakpam, Brinda Bhowmick, and Puspa Devi Pukhrambam

Abstract This chapter discusses the application of vertical tunnel FET (VTFET) as dielectric-modulated label-free biosensor. Various features of this biosensor are presented by focusing the analyses on enhancement of sensitivity, its lower limit of detection and response time. The concept of sensing is formulated on the dielectric modulation where the incubation of the biomolecules is represented by an insulator whose dielectric constant value is equal to the dielectric constant of target biomolecule since different biomolecules have unique dielectric constant. The proposed sensor design is deployed using a Technology Computer-Aided Design (TCAD) approach by incorporating relevant physics-based simulation models. Keeping in mind the practical consideration of the device, the study has been extended to analyze its performance under non-deal conditions like steric hindrance, irregular orientation. In the end, the status of the proposed sensor is highlighted by presenting the comparison of different sensing parameters of some significant work on TFET-based label-free biosensor available in the literature.

9.1 Introduction

The philosophy behind the Moore's law has been the guiding principle for the exponential growth of the semiconductor industries [1–3]. The continued scaling down of

V. D. Wangkheirakpam (✉) · B. Bhowmick · P. D. Pukhrambam
Department of Electronics and Communication, National Institute of Technology Calicut, Kozhikode, Kerala 673601, India
e-mail: vannawang46@gmail.com

B. Bhowmick
e-mail: bbhowmick@ece.nits.ac.in

P. D. Pukhrambam
e-mail: puspa.devi@ece.nits.ac.in

Department of Electronics and Communication, National Institute of Technology Silchar, Silchar, Assam 788010, India

© The Author(s), under exclusive license to Springer Nature Singapore Pte Ltd. 2023

G. Dutta and A. Biswas (eds.), *Next Generation Smart Nano-Bio-Devices*,
Smart Innovation, Systems and Technologies 322,
https://doi.org/10.1007/978-981-19-7107-5_9

the device dimension is performed to obtain good processing speed, low operating voltage and increase the number of transistors (MOSFETs) on chip so as to increase the device functionality [4, 5]. Scaling down of supply voltage leads to a reduction in dynamic power supply consumption which is desirable for power constraint applications. However, prolonged scaling down causes MOSFETs to encounter some serious issues known as the short channel effects (SCEs) [6–9]. Such issues arise due to the charge sharing between source and drain with the reduction in channel length, and as a result of this, various phenomenon such as velocity saturation, hot electron effects, DIBL effect are observed to be occurring [10–15]. Apart from these effects, the MOSFET technology faces another issue called the CMOS power problem. Decreasing the supply voltage (V_{DD}) at the time of scaling is required to maintain the power utilization of chip after the addition of a greater number of transistors [16–19]. But with the reduction of V_{DD}, the threshold voltage (V_{th}) should also be minimized in order to maintain the same ON state current, i.e., the overdrive voltage should be maintained. Therefore, to get the higher value of overdrive voltage, it is required to either keep V_{DD} at higher voltage or reduce V_{th} more forcefully [20–22]. The subthreshold swing (SS) of the state-of-the-art MOSFET cannot go down below 60 mV/dec due to its thermal limit, and this becomes a limiting factor of threshold voltage scaling. Also, keeping V_{DD} high leads to an increase in power consumption and thus causes the power crisis problem of CMOS. Hence, threshold voltage scaling can be done. In this scenario, it is found that tunnel field-effect transistor (TFET) has the ability to operate at low voltage with steeper SS and becomes a capable candidate which can replace MOSFETs in the near future. The fundamental fabrication methodologies of TFET are similar to MOSFET, and due to this, TFET has gained a concentrated focus for low applications as an alternative solution to scaled CMOS. Unlike the thermionic emission of MOSFETs, TFET conducts current through band-to-band tunneling (BTBT) mechanism resulting in low leakage current and steeper subthreshold swing [25, 26]. However, TFET experiences low ON state current and ambipolar behavior. Different modified structures of TFETs are proposed till now to overcome the limitation of conventional TFET geometry. Some of the widely used structures include heterojunction TFET, multiple gate TFET, III-V TFET, negative gate capacitance TFET, nanowire TFET, SOI TFET, etc.

TFETs are mostly popular for low-power digital circuits and memory applications. In the recent past, TFETs are observed to be widely used as a dielectrically modulated label-free biosensor. The sensitivity analysis is performed by observing the shift in drain current after the incubation of target molecules inside the sensing area. This current is affected by the dielectric constant and charge density of the target biomolecules. Section 9.2 of this chapter presents the concept of dielectric modulation in TFET, the geometry of TFET-based biosensor and its simulation strategies. Section 9.3 describes the proposed designed of VTFET biosensor. Section 9.4 discusses the sensitivity measurement methods. The non-idealities of TFET biosensors are analyzed in Sect. 9.5. Section 9.6 studies different sensing parameters considering the impact of charged biomolecules. Section 9.7 concludes the chapter.

9.2 Dielectric-Modulated Vertical TFET Biosensor: Concept, Geometry and Simulation Strategies

9.2.1 *Working Methodologies*

The conventional TFET has an insulator-gated reverse biased p-i-n geometry having three terminals, namely source, gate and drain. The source and drain regions are degenerated p and n-type, respectively. The channel remains intrinsic or doped lightly with p/n-type material, and it is sandwiched between the source and drain areas creating a p-i-n geometry. This arrangement provides a narrow depletion layer and forms a favorable condition for the carriers to tunnel from valence band (E_V) of source region to conduction band (E_C) of channel region. The fundamental working methodology of tunnel FET is Zener tunneling [27]. In TFET, BTBT is mechanism of electron transport. Depending on the polarity of the applied voltages, a TFET can be classified into p channel and n channel modes. In nTFET, the source terminal is connected to ground and the drain terminal is positively biased (V_{DS}) [28].

The application of positive voltage (V_{GS}) at the gate terminal causes band bending at the channel region. Further increase in this gate voltage causes more and more band bending resulting in the reduction of the tunneling width, i.e., the area between the E_V of source and E_C of channel where the bending is taken placed [29]. As V_{GS} increases beyond a particular limit known as the threshold voltage (V_{th}), carrier tunneling starts facilitating from the filled state E_V to the empty state Ec of source and channel, respectively. This can be understood from Fig. 9.1 where nature of E_C and E_V of the conventional TFET is plotted.

The tunneling probability of the energy barrier governs the current conduction of TFET. This probability is modeled through WKB approximation assuming a triangular barrier and is given by,

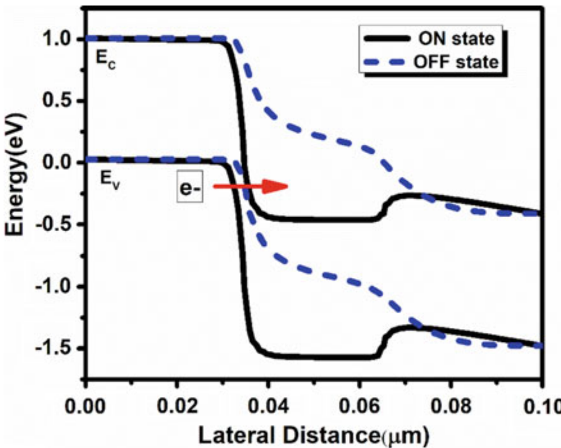

Fig. 9.1 Energy band diagram of nTFET showing the behavior at ON state and OFF state

$$T(E) = \exp\left(\frac{-4\lambda\sqrt{2m^*}E_g^{3/2}}{3q\hbar\left(E_g + \Delta\emptyset\right)}\right) \tag{9.1}$$

where m^* represents the effective mass, E_g denotes the forbidden energy gap, $\Delta\emptyset$ represents the energy of the area at tunnel junction where bands are overlapped, λ is the tunneling width, q and $\hbar$ are the value of an electronic charge and reduced Planck's constant, respectively. λ is defined as,

$$\lambda = \sqrt{\varepsilon_s/\varepsilon_{ox}t_{ox}t_s} \tag{9.2}$$

where $\varepsilon_s and \varepsilon_{\mathrm{ox}}$ correspond to the dielectric constants of substrate and oxide layer respectively, t_{ox} and t_s respectively represent the oxide and substrate thickness. It is clearly seen from Eqs. (9.1) and (9.2) that the drain current is a function of tunneling width whose value depends on material's dielectric constant (k). The gate and channel pairing are more for the higher value of k. This improves the tunneling probability giving higher value of I_D. The concept of dielectric modulation is applied in the TFET-based biosensors by incorporating embedded nanogaps at the regions above two junctions [30]. The drain current is found to be increasing when the analytes are incubated within the cavity regions due to the value of k possessed by the captured biomolecules. Drain current shift is measured to analyze the sensitivity of the sensor [32]. Different biomolecules have unique dielectric constant such as APTES = 3.57, uricase = 1.54, streptavidin = 2.1, protein = 2.5.

9.2.2 Geometry

As mentioned in previous section, the implementation of dielectric modulation in biosensing application requires the modification of the device geometry in order to incorporate a region where the molecules will be captured. The following are the fundamental requirements for such structural modification.

- The analytes should capture the target biomolecule and hybridized them in the region between the gate and channel acting like a gate dielectric. This can be realized by creating a nanogap after etching a part of the fixed dielectric material. The modified structure, therefore, has dual gate dielectric where one is the fixed high-k material (HfO2) and the other is the one possessed by the incubated biomolecules.
- The height nanogap cavities must be sufficient enough for the analyte to enter easily. In most of the analyses done for nanoscale TFET, this height is usually fixed at 10–15 nm.
- The structure can also be modified to increase the capture area of the biomolecules. This includes the utilization double gate and also creating nanogaps on either side of the fixed oxide layer.

- The structure must be designed in such a way that it can show significant change in the drain current even for low dielectric constant since some biomolecules have dielectric constants close to 2 or 3.
- The doping level of drain must be kept lesser than the source to prevent the ambipolarity effect to some extent.

9.2.3 Simulation Strategies

The dielectric-modulated biosensor can be conveniently analyzed on computational platform where the device architecture is employed with different physics-based models for its performance analyses. The simulation process is carried out using 2D Synopsys TCAD tool [31]. In the simulation process, the conditions when the cavities are incubated with target biomolecules are represented by an insulator with the same dielectric constant. For those biomolecules which carries charges, the impact of charge is taken in account by considering its effect at the oxide–semiconductor interface. Non-local band-to-band tunneling model is adopted to create the interband tunneling process as it looks after the gradient of the energy band as well. The bandgap narrowing model and Fermi–Dirac statistics are necessary since the geometries consist of highly doped source and drain. Field-dependent mobility models are also required.

9.3 Vertical TFET as Dielectric-Modulated Biosensor

This section presents a vertical TFET design for biosensing application and discusses some of its sensing parameters. This particular biosensor is designed using an n-type vertical tunnel FET (VTFET) via dielectrically modulated technology for label-free detection of biomolecules. The sensor design proposed in Fig. 9.2 is simulated in the Synopsys TCAD tool. An n+ pocket is incorporated in addition to the conventional design of TFET. This modification is done to boost the current when the device is in operation mode overcoming the limitation of conventional TFET. The SiGe pocket has 30% Ge concentration, and it is doped with 1×10^{19} cm^{-3} arsenic atoms. Another line tunneling normal to the gate stack is possible through this pocket in addition to the tunneling that occurs in the lateral direction resulting in enhanced drain current characteristics (I_D). Furthermore, the gate is modified by utilization dual metals with $\varphi_{m1} = 3.8$ eV (Al) near source end and $\varphi_{\mathrm{m2}} = 5.1$ eV (Au) near drain end. The arrangement is done to control the ambipolar behavior encounter in the TFET and also to improve the I_{ON}/I_{OFF} ratio. Source (p-type), i-channel and drain (n-type) have the doping concentration 5×10^{19} cm^{-3}, 1×10^{15} cm^{-3} and 1×10^{18} cm^{-3}, respectively. The 10 nm long and 10 nm high HfO2 is kept as a constant dielectric material. The presence of nanogaps on both side of this fixed oxide allows incubation of more molecules inside the cavity. An SiO2 layer with

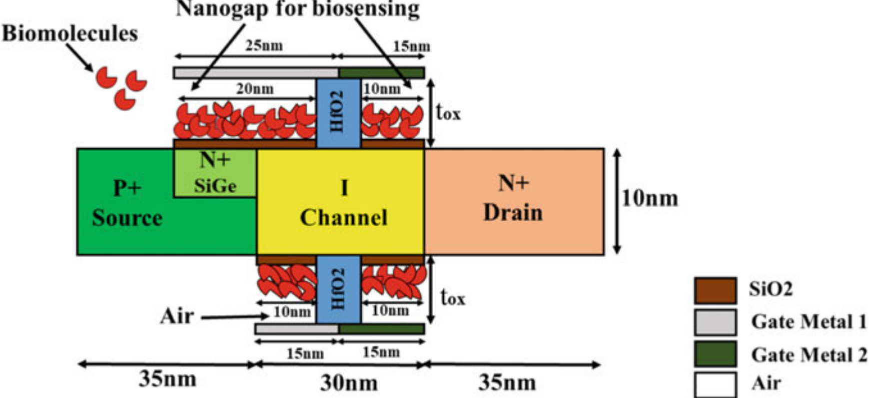

Fig. 9.2 Schematic image of n-VTFET biosensor

thickness 1 nm is introduced within the cavities representing the glass slides where the receptor molecules are immobilized, and this also minimizes the leakage current and degradation of sensitivity. The entire process of detection is considered to occur in a dry environment.

9.4 Sensitivity Measurement

The most common method of analyzing the sensitivity is the measurement of the change in its electrical parameters. Sensitivity calculation based on the change in drain current and threshold voltage is used as the most convenient technique. The sensitivity of the sensor is measured with reference to the value of the desired electrical parameter obtained when the nanogap is devoid of biomolecules, i.e., assuming that it is occupied by air ($k = 1$). The mathematical formula for the calculation of drain current sensitivity at fixed gate bias is given by,

$$\text{Sensitivity, } S_I = \left.\frac{I_{D(k=\text{BIO})}}{I_{D(k=\text{AIR})}}\right|_{V_{\text{GS}}} \tag{9.3}$$

where $I_{D(k=\text{BIO})}$ and $I_{D(k=\text{AIR})}$ respectively represent the value of drain current for the filled state and empty state. The threshold voltage (V_{th}) of a device is also a function of dielectric constant and oxide–semiconductor interface charges. Hence, V_{th} can also be used as a parameter for measuring the sensitivity. The mathematical relation is

$$\text{Sensitivity, } S_{V_{\text{th}}} = V_{\text{th}(k=\text{AIR})} - V_{\text{th}(k=\text{BIO})} \tag{9.4}$$

where $V_{th(k = AIR)}$ and $V_{th(k = BIO)}$ respectively define the threshold voltage at empty state and filled state. It is possible to extract V_{th} in a numerous way using transfer characteristics curve. The most commonly used methods are constant current method and the linear extrapolation (LE) method.

9.5 Non-ideal Hybridization of Biomolecules Inside the Nanogaps

In the simulation process, it is favorable to consider the nanogaps are completely filled with the analytes. However, in practice, this assumption is not always true. The conditions like steric hindrance and irregular orientation of receptors/probe are resulting in different partially filled profiles of the nanogaps.

9.5.1 Steric Hindrance

Steric hindrance is the condition arises when already hybridized biomolecules restrict the entry of the new one before the cavities are completely filled. This results in a different cavity profile and consequently alters the sensitivity. This partial hybridization condition is implemented in the TCAD simulation process by considering step profiles including increasing, decreasing, concave and convex. This is designed by defining various height of the dielectric material inside the nanogaps mimicking the pattern of partially filled molecules as shown in Fig. 9.3.

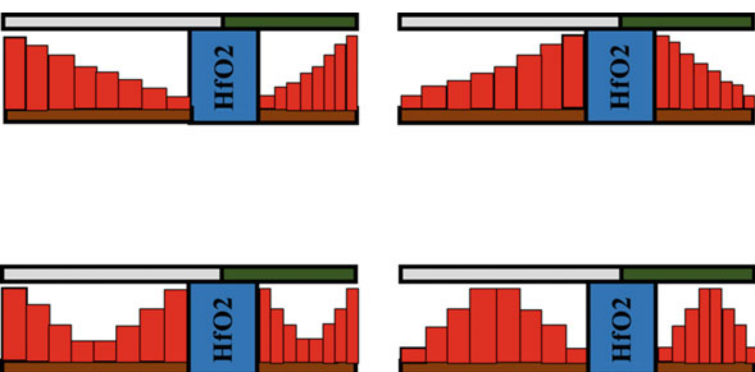

Fig. 9.3 Probable step profiles of the cavity introduce due to the steric hindrance

9.5.2 Receptor Placement

The receptors or probes are immobilized on the sensing surface usually a glass slide in order to capture the target biomolecule and hybridized them inside the cavity. The receptor molecules have an antigen binding site which will recognize the target biomolecule. If these receptor molecules are not properly aligned, then it will not be able to capture the antibody. This may result in the partially filled cavity profiles. Also, the placement of these receptors may not be continued throughout the cavity. In the simulation process, this is defined by inserting air gaps in between the insulators representing the biomolecules.

9.6 Sensing Parameters of VTFET Biosensor

This section observes the influence of different factors like charged molecules, step profiles, etc. on the sensitivity of the VTFET biosensor. Other sensing parameters such response time and lower limit of detection are also discussed in this section.

9.6.1 Biomolecules Carrying Negative Charge

It is known that the sensitivity is altered by the charges of the biomolecule. Assuming the nanogaps to be fully filled, the impact of the magnitude of negative charges on the sensitivity of the VTFET biosensor is investigated for four different values of k (5, 7, 10 and 12) representing four different biomolecules. The result shown in Fig. 9.4a provides the gradual degradation of sensitivity as the number of negative charges rises. The negative charges of the biomolecules present near the SiO2 surface prevent the further depletion of the p-type channel thereby increasing the V_{GS} needed for channel inversion. This can be explicated using the following equation.

$$V_G = \Psi_S + \Phi_{\mathrm{MS}} - \frac{qN_{\mathrm{bio}}}{C_{\mathrm{ox}}} \tag{9.5}$$

Since the sensitivity is measured at fixed V_{GS} and V_{DS}, the potential balance equation given in Eq. (9.5) will be satisfied only if the value of Ψ_S is reduced as the magnitude of negative charge increases. Accordingly, the drain current degrades giving reduced sensitivity. Figure 9.4a also demonstrates the increase in sensitivity with k value. This is due the increase in the gate-channel coupling as the value of k increases. Figure 9.4b depicts the I_D-V_{GS} characteristics visualizing the impact of positive and negative charges of the analytes incubated inside the nanogap cavities. It is evident that the curve shifts upward as the value of charges changes from extreme negative to the extreme positive. The curve for $k = 1$ represents the result obtain when

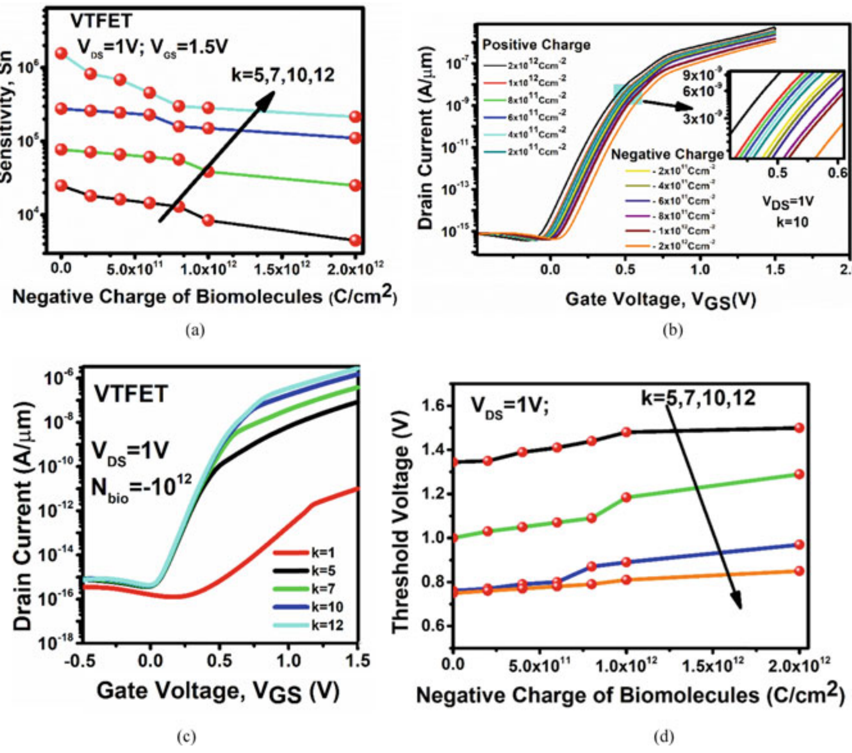

Fig. 9.4 **a** Sensitivity variation plot due to the influence of biomolecules carrying negative charge, **b** transfer characteristics curves showing the impact of various negative and positive charges, **c** I_D-V_{GS} curve of VTFET biosensor for $k = 1, 5, 7, 10$ and 12 at $N_{bio} = -10^{12}$ C/cm^2, **d** V_{th} versus negative charge of biomolecules at $k = 5, 7, 10$ and 12

the nanogap is devoid of biomolecules, i.e., the condition when it is filled with air. The presence of nanogaps on either side of the fixed dielectric (HfO2) increases the area where the target biomolecules can be captured. Figure 9.4c shows the I_D-V_{GS} curve of VTFET biosensor for $k = 1, 5, 7, 10$ and 12 at fixed negative charge $N_{bio} = -10^{12}$ C/cm^2. The shift in drain current as an after effect of the impact of charge density impact also explains the change in threshold voltage. The threshold voltage obtain for each case is plotted in Fig. 9.4c. V_{th} increases as the magnitude of negative charges increases.

9.6.2 Biomolecules Carrying Positive Charge

Similar to Sec. 9.6.1, various plots for positive charge biomolecules are presented in this section. Figure 9.5a shows the sensitivity plot for various magnitude of positive charges. The biomolecules possessing positive charge which are present at the interface enhance the depletion of channel and improve the quantum mechanical tunneling of electron. As a result, the sensitivity rises. The trend of plots is analogous to Sect. 9.6.1. Figure 9.5b shows the I_D-V_{GS} curve of the VTFET biosensor for various value of at $N_{bio} = 10^{12}$ C/cm^2. The corresponding threshold voltage for each value of positive charge density is plotted in Fig. 9.5c.

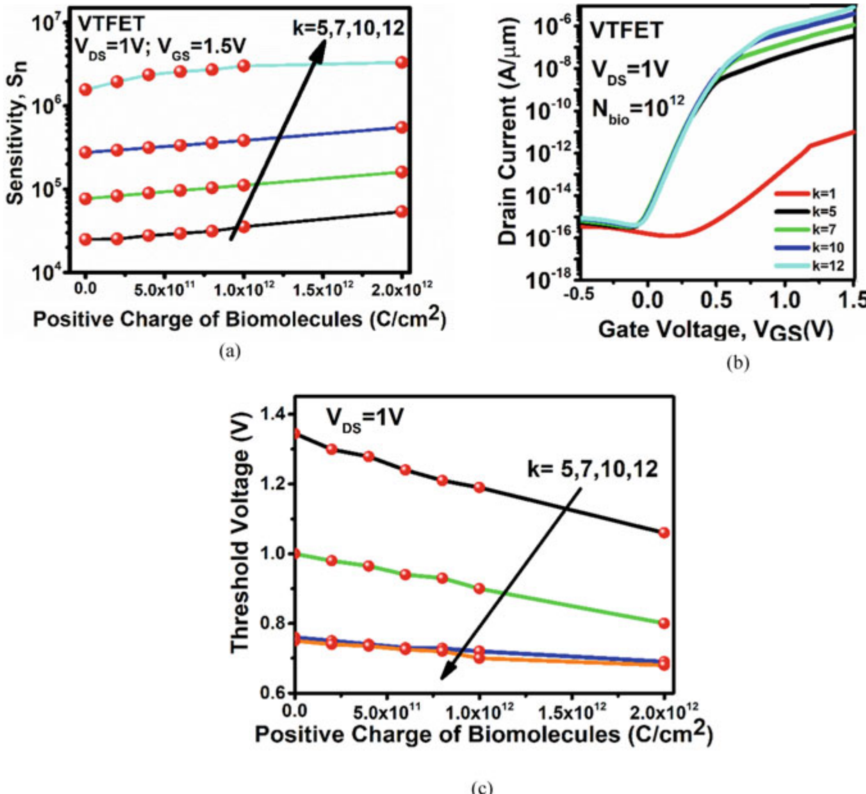

Fig. 9.5 **a** Sensitivity obtained at various positive charge densities of the biomolecules **b** I_D-V_{GS} curve of VTFET biosensor for $k = 1, 5, 7, 10$ and 12 at $N_{bio} = 10^{12}$ C/cm^2, **c** V_{th} versus positive charge densities of the biomolecules

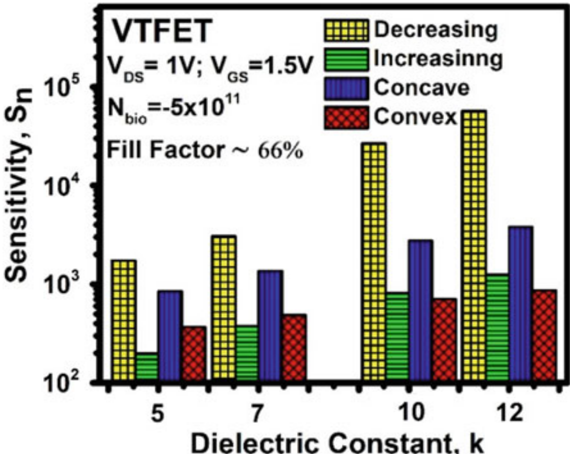

Fig. 9.6 Sensitivities of different step profiles of the biomolecules inside the nanogaps of VTFET biosensor

9.6.3 Step Profiles of Biomolecules Inside the Nanogaps

The comparison of the sensitivities for four different step profiles of biomolecules, viz., increasing, decreasing, concave and convex is shown in Fig. 9.6. Due to the steric hindrance, only 66% of nanogaps are occupied by biomolecules. The decreasing and concave profile response well, but the remaining two show very less sensitivity. This is because the decreasing and concave profile have highest steps close to the source-channel junction where tunneling takes place. Whereas in case of increasing and convex profiles, the highest step lies farther from the tunneling junction and this reduces the gate-channel coupling.

9.6.4 Response Time and Lower Limit of Detection

The time taken to rise to 90% of final value measured from onset of step input change is defined as the time response. The response time of VTFET biosensor is measured from Fig. 9.7a, and it is found to be $t_{pLH} = 12$psec. Thus, this biosensor has very less response time which means it will response faster. This is because of the steeper SS characteristics of TFET.

The lower limit of detection (LOD) is calculated from the signal-to-noise ratio (SNR) measured using a combination of noise and *I*-*V* characterization. The SNR for FET-based biosensor in terms of number fluctuation model is presented as [33],

$$\mathrm{SNR} = \frac{g_m}{\sqrt{S_{\mathrm{id}}}} = \frac{1}{\sqrt{S_{VFB}}} = \sqrt{\frac{WLC_{\mathrm{ox}}^2 f}{\lambda kTq^2 N_T}} \tag{9.6}$$

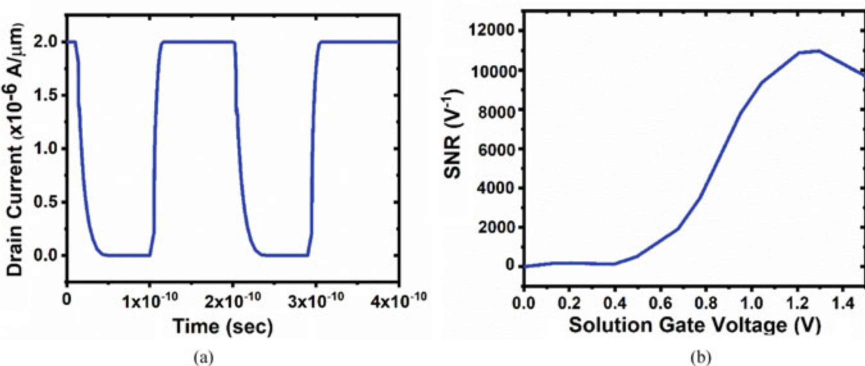

Fig. 9.7 **a** Drain current response w.r.t. time of VTFET biosensor at $k = 12$, **b** SNR versus solution gate voltage

where W and L respectively represent the width and length. T is the temperature, λ is the tunneling parameter, f is the frequency at which noise density power ($S_{\rm id}$) is evaluated, and $C_{\rm ox}$ gives the oxide capacitance. Density of trap states such as interface traps/defects and surface states is given by N_T. In dielectric-modulated FET biosensors, the LOD is obtained by measuring the minimum change in the surface potential that can be detected which is obtained from 1/SNR. This value is restricted by the fluctuation in flat-band voltage caused by the traps and interface states [33]. Figure 9.7b shows the SNR plot with respect to the applied gate voltage. The value of peak SNR is 11200 which interprets to a minimum detectable voltage of ~89 μV. Hence, for this significantly low minimum detectable voltage, the LOD obtain is significantly less.

9.6.5 Status of VTFET Biosensor

This section shows the status of VTFET biosensor among various simulated, analytically modeled and fabricated FET-based biosensors available in the literature. Table 9.1 presents the sensitivity comparison of various geometries of DM TFET biosensors and highlights the status of the proposed VTFET biosensor.

9.7 Conclusion

This chapter presents a brief idea of the application of TFETs as dielectrically modulated label-free biosensor. Various aspects of TFET-based biosensor are studied through TCAD simulation with main focus on design and development of higher sensitivity sensor. The study has been extended to analyze the practicality of the

Table 9.1 Overview of various TFET-based biosensors

S. No.	Biosensors	Approx. sensitivity	ΔP
1	Conventional TFET [17]	50	12.5
2	Nanowire TFET [17]	9×10^3	2.25×10^3
3	DM FET ($L_{gap} = 200$ nm, $H_{gap} = 15$ nm, $k = 2.1$) [18]	1×10^4	2.5×10^3
4	DM FET ($L_{gap} = 100$ nm, $H_{gap} = 15$ nm, $k = 2.1$) [18]	3×10^4	7.5×10^3
5	Lateral DM TFET ($L_{gap1} = 10$ nm, $H_{gap} = 5$ nm, $k = 2$) [23]	10	2.5
6	Vertical DM TFET ($L_{gap1} = 10$ nm, $L_{gap2} = 15$ nm $H_{gap} = 5$ nm, $k = 2$) [23]	40	10
7	Full gate DM TFET ($L_{gap} = 10$ nm, $H_{gap} = 5$ nm, $L_{gate} = 42$ nm, $k = 4$) [19]	1×10^5	2.5×10^4
8	Short gate DM TFET ($L_{gap} = 10$ nm, $H_{gap} = 5$ nm, $L_{gate} = 20$ nm, $k = 4$) [19]	1×10^6	2.5×10^5
9	DM FET ($L_{gap} = 30$ nm, $L_{gate} = 100$ nm, $H_{gap} = 9$ nm, $k = 10$)[20]	5	1.25
10	DM FET ($L_{gap} = 75$ nm, $L_{gate} = 250$ nm, $H_{gap} = 9$ nm, $k = 10$) [20]	7	1.4
11	DM PNPN TFET ($L_{gap} = 30$ nm, $L_{gate} = 100$ nm, $H_{gap} = 9$ nm, $k = 10$) [20]	3×10^6	7.5×10^5
12	SiGe source DM PNPN TFET with 0% Ge composition ($L_{gap} = 15$ nm, $L_{gate} = 100$ nm, $H_{gap} = 9$ nm, $k = 2.1$) [22]	4×10^3	1×10^3
13	SiGe source DM PNPN TFET with 10% Ge composition ($L_{gap} = 15$ nm, $L_{gate} = 100$ nm, $H_{gap} = 9$ nm, $k = 2.1$) [22]	6×10^3	1.5
14	SiGe source DM PNPN TFET with 20% Ge composition ($L_{gap} = 15$ nm, $L_{gate} = 100$ nm, $H_{gap} = 9$ nm, $k = 2.1$) [22]	5×10^3	1.25×10^3
15	Dual metal gate SiGe pocket vertical TFET ($L_{gap1} = 20$ nm, $L_{gap2} = 10$ nm $H_{gap} = 5$ nm, $L_{gate1} = 25$ nm, $L_{gate1} = 15$ nm, $k = 12$) [This work]	2×10^6	5×10^5

Sensitivity of biosensor = (ΔP × Sensitivity of MOSFET-based biosensor)
Approximate sensitivity of MOSFET-based biosensor [24] = 4

sensor by considering some non-idealities. A vertical tunnel FET-based biosensor is proposed in this chapter, and it shows interesting results in terms of sensitivity, response time and lower limit of detection. Eventually, an overview of various FET sensors is presented to highlight the status of the VTFET biosensor.

References

1. Barbaro, M., Bonfiglio, A., Raffo, L.: A charge-modulated FET for detection of biomolecular processes : conception. **53**(1), 158–166 (2006)
2. Kim, C.-H., Jung, C., Park, H.-G., Choi, Y.-K.: Novel dielectric- modulated field-effect transistor for label-free DNA detection. Biochip J. **2**(2), 127–134 (2008)
3. Wangkheirakpam, V.D., Bhowmick, B., Pukhrambam, P.D.: Near-infrared optical sensor based on band-to-band tunnel FET. Appl. Phys. A **125**(341), 1–9 (2019). https://doi.org/10.1007/s00339-019-2636-3
4. Chanda, M., Das, R., Kundu, A., Sarkar, C.K.: Analytical modeling of label free biosensor using charge plasma based gate underlap dielectric modulated MOSFET. Superlattices Microstruct. **104**, 451–460 (2017). https://doi.org/10.1016/j.spmi.2017.03.010
5. Narang, R., Saxena, M., Gupta, R.S., Gupta, M.: Dielectric modulated tunnel field-effect transistor—A biomolecule sensor. IEEE Electron Device Lett. **33**(2), 266–268 (2012). https://doi.org/10.1109/LED.2011.2174024
6. Choi, M., Han, J.-W., Choi, S.-J., Choi, Y.-K.: Analytical modeling of a nanogap-embedded FET for application as a biosensor. IEEE Trans. Electron Devices **57**(12), 3477–3484 (2010). https://doi.org/10.1109/TED.2010.2076152
7. Kannan, N., Kumar, M.J.: Charge-modulated underlap I-MOS transistor as a label-free biosensor: a simulation study. IEEE Trans. Electron Devices **62**(8), 2645–2651 (2015). https://doi.org/10.1109/TED.2015.2446612
8. Shan, C., Wang, Y., Bao, M.-T.: A charge-plasma-based transistor with induced graded channel for enhanced analog performance. IEEE Trans. Electron Devices **63**(6), 2275–2281 (2016). https://doi.org/10.1109/TED.2016.2549554
9. Das, R., Chanda, M., Sarkar, C.K.: Analytical modeling of charge plasma-based optimized nanogap embedded surrounding gate MOSFET for label-free biosensing. IEEE Trans. Electron Devices **65**(12), 5487–5493 (2018). https://doi.org/10.1109/TED.2018.2872466
10. Narang, R., Reddy, S., Saxena, M., Gupta, R. S., Gupta, M.: A dielectric-modulated tunnel-FET-based biosensor for label-free detection: analytical modeling study and sensitivity analysis. IEEE Trans. Electron Devices **59**(10), 2809–2817 (2012). https://doi.org/10.1109/TED.2012.2208115
11. Dutta, R., Sarkar, S.K.: Analytical modeling and simulation-based optimization of broken gate TFET structure for low power applications. IEEE Trans. Electron Devices **66**(8), 3513–3519 (2019). https://doi.org/10.1109/TED.2019.2925109
12. Choi, W.Y., Park, B., Lee, J.D., Liu, T.K.: Tunneling field-effect transistors (TFETs) with subthreshold swing (SS) less than 60 mV/dec. IEEE Electron Device Lett. **28**(8), 743–745 (2007)
13. Bhuwalka, K.K., Sedlmaier, S., Ludsteck, A.K., Toksdorf, C., Schulzeand, J., Eisele, I.: Vertical tunnel field-effect transistor. IEEE Trans. Electron Devices **51**(2), 279–282 (2004). https://doi.org/10.1109/TED.2003.821575
14. Wirths, S., Tiedemann, A.T., Trellenkamp, S., Buca, D., Zhao, Q.T., Mantl, S.: Novel SiGe/Si line tunneling TFET with high Ion at low VDD and constant SS. In: Proc. IEDM, pp. 608–611 (2015). https://doi.org/10.1109/IEDM.2015.7409757
15. Huang, Q., Huang, R., Wu, C., Zhu, H., Chen, C., Wang, J., Guo, L., Wang, R., Ye, L., Wang, Y.: Comprehensive performance reassessment of TFETs with a novel design by gate and source engineering from device/circuit perspective. In: Proc. IEDM, pp. 335–338. (2014). https://doi.org/10.1109/IEDM.2014.7047044
16. Zhou, G., Li, R., Vasen, T., Qi, M., Chae, S., Lu, Y., Zhang, Q., Zhu, H., Kuo, J.-M., Kosel, T., Wistey, M., Fay, P., Seabaugh, A., Xing, H.: Novel gate-recessed vertical InAs/GaSb TFETs with record high I_{ON} of 180μA/μm at VDS = 0.5 V. In: Proc. IEDM, pp. 777–780 (2012). https://doi.org/10.1109/IEDM.2012.6479154
17. Devi, W.V., Bhowmick, B.: Optimisation of pocket doped junctionless TFET and its application in digital inverter. Micro Nano Lett. 1–5 (2018). https://doi.org/10.1049/mnl.2018.5086

18. Gao, A., Lu, N., Wang, Y., Li, T.: Robust ultrasensitive tunnelling FET biosensor for point-of-care diagnostics. Sci. Rep. **6**, 22554 (2015)
19. Pratap, Y., Kumar, M., Kabra, S., et al.: Analytical modeling of gateall-around junctionless transistor based biosensors for detection of neutral biomolecule species. J. Comput. Electron. **17**(1), 288–296 (2017)
20. Verma, M., Tirkey, S., Yadav, S., Sharma, D., Yadav, D.S.: Performance assessment of a novel vertical dielectrically modulated TFET-based biosensor. IEEE Trans. Electron Devices **64**(9), 3841–3848 (2017)
21. Van Haaften, A.B.: Acute Tetrabromoethane (Acetylene Tetrabromide) Intoxication in Man. Am. Ind. Hyg. Assoc. J. **30**(3), 251–256 (1969)
22. Xu, R.: In: Brian Scarlett (ed.) Particle Characterization: Light Scattering Methods (2002)
23. Sarkar D., Banerjee, K.: Proposal for tunnel-field-effect- transistor as ultra-sensitive and label-free biosensors. Appl. Phys. Lett. **100**(14) (2012)
24. Wangkheirakpam, V.D., Bhowmick, B., Pukhrambam, P.D.: N+ pocket doped vertical TFET based dielectric-modulated biosensor considering non-ideal hybridization issue: a simulation study. IEEE Trans. Nanotechnol. **19**, 156–162 (2020). https://doi.org/10.1109/TNANO.2020.2969206
25. Wangkheirakpam, V.D., Bhowmick, B., Pukhrambam, P.D.: N+ pocket-doped vertical TFET for enhanced sensitivity in biosensing applications: modeling and simulation. IEEE Trans. Electron Devices **67**(5), 2133–2139 (2020). https://doi.org/10.1109/TED.2020.2981303
26. Wangkheirakpam, V.D., Bhowmick, B., Pukhrambam, P.D.: Modeling and simulation of optically gated TFET for near infra-red sensing applications and its low frequency noise analysis. IEEE Sens. J. **20**(17), 2133–2139 (2020). https://doi.org/10.1109/JSEN.2020.2991406
27. Narang, R., Saxena, M., Gupta, R.S., Gupta, M.: Comparative analysis of dielectric- modulated FET and TFET-based biosensor. IEEE Trans. Nanotechnol. **14**(3), 427–435 (2015)
28. Kanungo, S., Chattopadhyay, S., Gupta, P.S., Sinha, K., Rahaman, H.: Study and analysis of the effects of SiGe source and pocket-doped channel on sensing performance of dielectrically modulated tunnel FET-based biosensors. IEEE Trans. Electron Devices **63**(6), 2589–2596 (2016)
29. Goswami, R., Bhowmick, B.: Comparative analyses of circular gate TFET and heterojunction TFET for dielectric—modulated label—free biosensing. IEEE Sens. J. **PP**(1), 1 (2019)
30. Bhattacharyya, A., Chanda, M., De, D.: Performance assessment of new dual-pocket vertical heterostructure tunnel FET-based biosensor considering steric hindrance issue. IEEE Trans. Electron Devices **66**(9), 3988–3993
31. TCAD Sentaurus Device User's Manual, Synopsys, Inc., Mountain View, CA, USA (2010)
32. Wangkheirakpam, V.D., Bhowmick, B., Pukhrambam, P.D.: Detection of SARS-CoV-2 using dielectric modulated TFET based biosensor. J. Mater. Sci. Mater. Electron. 1–12. https://doi.org/10.1007/s10854-022-08020-3
33. Rajan, N.K., Brower, K., Duan, X., Reed, M.A.: Limit of detection of field effect transistor biosensors: effects of surface modification and size dependence. Appl. Phys. Lett. **104**, 084106–084111 (2014). https://doi.org/10.1063/1.4867025